Arsenic mobilization in a seawater inundated acid sulfate soil

Johnston, Scott G; Keene, Annabelle F; Burton, Edward D; Bush, Richard T; et al.

Johnston, S. G., Keene, A. F., Burton, E. D., Bush, R. T., Sullivan, L. A., McElnea, A. E., Ahern, C. R., Smith, C. D., Powell, B., & Hocking, R. K. (2010). Arsenic mobilization in a seawater inundated acid sulfate soil. Environmental Science and Technology, 44(6), 1968–1973. https://researchportal.scu.edu.au/esploro/outputs/journalArticle/Arsenic-mobilization-in-a-seawater-inundated/991012821452602368

Original article published as: Johnston S.G., Keene A.F., Burton E.D., Bush R.T., Sullivan L.A., McElnea A.E., Ahern C.R., Smith C.D., Powell B. (2010) Arsenic mobilisation in a seawater inundated acid sulfate soil. *Environmental Science and Technology* 44 (6), 1968–1973.

Arsenic mobilization in a seawater inundated acid sulfate soil

Scott G. Johnston[A]*, Annabelle F. Keene[A], Edward D. Burton[A], Richard T. Bush[A], Leigh A. Sullivan[A], Angus E. McElnea[B], Col R. Ahern[B], C. Douglas Smith[B], Bernard Powell[B], Rosalie K. Hocking[C]

*Corresponding author (Scott G Johnston: scott.johnston@scu.edu.au)

[A]Southern Cross GeoScience
Southern Cross University, Lismore, NSW 2480, Australia

[B]Department of Environment and Resource Management, 80 Meiers Road, Indooroopilly, Qld. 4068, Australia

[C]Monash Centre for Synchrotron Science and School of Chemistry
Monash University, Clayton, Vic. 3800, Australia.

Abstract

Tidal seawater inundation of coastal acid sulfate soils can generate Fe- and SO_4-reducing conditions in previously oxic-acidic sediments. This creates potential for mobilization of As during the redox transition. We explore the consequences for As by investigating the hydrology, porewater geochemistry, solid-phase speciation and mineralogical partitioning of As across two tidal fringe toposequences. Seawater inundation induced a tidally-controlled redox gradient. Maximum porewater As (~400 μg/L) occurred in the shallow (<1 m), intertidal, redox transition zone between Fe-oxidizing and SO_4-reducing conditions. Primary mechanisms of As mobilization include the reduction of solid-phase As(V) to As(III), reductive dissolution of As(V)-bearing secondary Fe(III) minerals and competitive anion desorption. Porewater As concentrations decreased in the zone of contemporary pyrite reformation. Oscillating hydraulic gradients caused by tidal pumping promote upward advection of As and Fe^{2+}-enriched porewater in the intertidal zone, leading to accumulation of As(V)-enriched Fe(III) (hydr)oxides at the oxic sediment-water interface. Whilst this provides a natural reactive-Fe barrier, it does not completely retard the flux of porewater As to overtopping surface waters. Furthermore, the accumulated Fe minerals may be prone to future reductive dissolution. A conceptual model describing As hydro-geochemical coupling across an intertidal fringe is presented.

Keywords: Acid sulfate soil; Arsenic; Iron; Sea-level rise; Subterranean estuary; Tidal marsh; Wetland; East Trinity

Cite as: Johnston S.G., Keene A.F., Burton E.D., Bush R.T., Sullivan L.A., McElnea A.E., Ahern C.R., Smith C.D., Powell B. (2010) Arsenic mobilisation in a seawater inundated acid sulfate soil. *Environmental Science and Technology* 44 (6), 1968–1973

Introduction

Arsenic is an important contaminant in coastal floodplain aquifers which degrades the health of millions of people (*1*). It is increasingly recognized that As can be mobilized during redox transitions caused by inundation of oxic sediments (*2*−*4*). The mechanisms of As mobilization and attenuation in coastal aquifers are complex, yet are often intimately coupled with the geochemical cycling of Fe (hydr)oxides and sulfide minerals (*5*−*8*).

Acid sulfate soils form on coastal floodplains due to pyrite oxidation. They occupy over 12 million ha globally (*9*) and often have elevated concentrations of As due to the tendency of As to accumulate in pyrite (*1*). Acid sulfate soils are also usually rich in secondary Fe(III) minerals such as goethite (α-FeOOH), ferrihydrite ($Fe_5O_3(OH)_9$), jarosite ($KFe_3(SO_4)_2(OH)_6$), and schwertmannite ($Fe_8O_8(OH)_6SO_4$) (*10*). These Fe(III) minerals are important sorbents for As and can become enriched in As under oxic conditions in both acid sulfate soils and acid mine drainage (*1, 4, 11*−*15*). Most studies of As behavior in coastal acid sulfate soils (CASS) have focused on oxidative pathways of mobilization (*16*−*18*), with reductive mobilization only recently investigated (*3*). This is surprising given that many CASS landscapes experience seasonally fluctuating water tables and undergo cyclic redox transformations (*19*).

Recently, seawater inundation has been used as a technique for successfully ameliorating acidity within lowland CASS (*20*−*22*). Seawater inundation initiates a large redox transition which leads to reductive dissolution of Fe(III) minerals, SO_4^{2-} reduction and the reformation of sulfide-minerals, including pyrite (*21*). It also introduces tidal pumping to shallow groundwater, which can cause porewater exchange and solute redistribution within intertidal zone sediments (*23, 24*).

There is an as yet unexamined potential for As mobilization and hydro-geochemical coupling with Fe and S across seawater inundation induced redox boundaries in CASS. It is important to understand the landscape-scale behavior of As in this context for several reasons. First, in order to evaluate the geochemical consequences of seawater inundation as a remediation strategy for CASS. Second, large areas of CASS are <1 m above current sea-level and therefore at risk of increasing tidal inundation due to future sea-level rise (*25*).

This study investigates As mobilization, redistribution, and attenuation in a seawater-inundated CASS landscape. We aim to quantify the in situ solid- and aqueous-phase distribution, speciation, and mineralogical partitioning of As across two tidal toposequences. We also present a conceptual model of As hydro-geochemical zonation that is applicable to seawater-inundated CASS.

Materials and Methods

Study Site. The study site is a ~200 ha subcatchment of a Holocene sedimentary coastal plain in tropical northern Australia (Figure SI1 of the Supporting Information). A tide-excluding sea wall was constructed around the site in the 1970s (*20*). Tide exclusion combined with intensive drainage caused the oxidation of iron-sulfides in mangrove sediments, leading to widespread formation of severe acid sulfate soils across the site (*20, 26*). A remediation program commenced in 2001−02, which has involved incrementally increasing tidal inundation of acid sulfate soils up to an elevation of ~0.5 m AHD (AHD is Australian height datum, 0 m AHD approximates mean sea level) (*20*). The site is close to a large bay, and tidal waters are strongly marine for most of the year (*27*). Tides now regularly inundate most of the formerly acidified areas across the site. This approach has led to substantial decreases in soil and water acidity and has stimulated extensive Fe- and SO_4^{2-}-reduction (*21, 27*).

Two toposequence transects were established to bracket the fringe of the tide-imposed redox gradient (i.e., spanning the supratidal/intertidal zone; 0.6−0 m AHD; Figure 1, Figure SI2 of the Supporting Information). Both transects have similar stratigraphy (derived from coring) and are comprised of clay-textured former sulfuric horizons to about 0.7−1.0 m below ground level (bgl), underlain by unoxidized, sulfidic estuarine muds. Former sulfuric horizons contain relict jarosite pedofeatures typical of acid sulfate soils and were classified as Hydraquentic Sulfaquepts (*21*) prior to inundation with seawater.

Hydrology. Details of hydrological assessments are described in the Supporting Information. In brief, groundwater levels along each transect were measured at 30 min intervals (±0.01 m) using submersible pressure transducers vented to the atmosphere (Odyssey, ODYPS05) housed in a series of four 50 mm diameter PVC piezometers. All levels are reported in AHD.

Solid-Phase Sampling and Characterization. Four replicate soil cores were obtained by 1.5 m gouge-auger from each sampling location at Transect 1 during April 2008 and Transect 2 during October 2007. Cores were immediately sectioned, and subsamples from equivalent depths were combined in approximately equal quantities to decrease variation arising from spatial heterogeneity. Samples were sealed in airtight polyethylene bags, completely filled with soil and frozen within ~6 h of collection until analysis. Soil pH (pH_F) and redox potential (Eh_F) were determined in the field on additional duplicate cores by direct insertion of freshly calibrated electrodes. Fe-rich surficial sediment (0−0.01 m) was also sampled from a variety of locations within the study area and frozen. The elevation of all sample points was surveyed to AHD. Further detail on solid-phase sampling can be found in the Supporting Information.

Samples were thawed under N_2, homogenized, and analyzed in duplicate for reactive Fe fractions and speciation. Poorly crystalline solid-phase Fe(II) and Fe(III) were extracted with 0.5 M HCl on 1−2 g wet subsamples which enables preservation of redox speciation (*28, 29*). Aliquots of 0.45 μm-filtered extract were analyzed for Fe(II) [$Fe(II)_{HCl}$] and total Fe [Fe_{HCl}] by the 1,10-phenanthroline method (*30*) with Fe(III) determined by difference. The centrifuged residue was then extracted with a citrate-buffered dithionite solution [Fe_{DCb}] (*28*), which leaches more crystalline forms of Fe including lepidocrocite and goethite (*28, 31*). The sum of Fe_{HCl} and Fe_{DCb} is reported as Fe_R and largely represents the Fe pool available for reductive transformations over biologically relevant time scales.

Soil moisture content (θ) was determined by weight loss after oven drying a subsample at 105 °C. A separate portion of sample was dried at 85 °C and crushed to pass a 0.5 mm sieve. These dried and crushed samples were analyzed via the chromium reduction technique [S_{CR}] (*32*). Total organic carbon (TOC) was determined by combustion (LECO CNS-2000) after HCl treatment. Near-total As [As_{Tot}] was extracted by hot aqua-regia digestion (*30*) and measured by ICP-MS (Perkin-Elmer ELAN-DRCe). HCl-extractable As [As_{HCl}] was determined on 0.45 μm-filtered aliquots derived from Fe_{HCl} extracts and measured by ICP-MS. Duplicate analysis performed on 12% of samples had a precision within 8%. Water-soluble Cl and S was determined on a 0.45 μm-filtered aliquots of 1:5 soil:water extracts via by flow injection analysis (Lachat QuikChem 8000) and ICP-AES (Perkin-Elmer DV4300) respectively.

Cite as: Johnston S.G., Keene A.F., Burton E.D., Bush R.T., Sullivan L.A., McElnea A.E., Ahern C.R., Smith C.D., Powell B. (2010) Arsenic mobilisation in a seawater inundated acid sulfate soil. *Environmental Science and Technology* 44 (6), 1968–1973

Jarosite pedofeatures from former sulfuric horizons were removed with a scalpel from air-dried bulk soil under a light microscope. Pyrite was collected from a bulk sample (~0.5 kg) of unoxidised sulfidic sediment by density separation with *s*-tetrabromoethane (*33*). Selected samples were examined via XRD using a Bruker D4 Endeavor fitted with a Co X-ray source and Lynx-Eye detector. Samples were scanned from 15°− 80° 2θ with a 0.05° 2θ step-size and a 4 s count-time and analyzed using EVA software (DIFFRAC-plus evaluation package, Bruker AXS, Karlsruhe, Germany).

Arsenic K-edge X-ray absorption near-edge structure (XANES) spectra were collected on bending magnet beamline 20B at the Photon Factory, Tsukuba Japan. The X-ray energy resolution was maintained by a Si(111) channel-cut monochromator, and the energy was calibrated against the first inflection point of $Na_2HAs^VO_4$. Natural sediment samples were placed under Kapton tape and held at 10−15 K with a He cryostat to avoid changes in oxidation state. Duplicate spectra were collected in fluorescence mode using a 32 element array Ge solid-state detector and averaged. The spectral background was subtracted using a polynomial fit, and the edge jump height was normalized to unity using PySpline software (*34*). The oxidation state of As in samples was determined by comparison to the XANES edge position of selected reference standards. While our standards data show broadening consistent with self-absorption, they are sufficient to determine the energy positions associated with As oxidation states.

Porewater Geochemistry. Porewaters were sampled during April 2008 via equilibration dialysis, described in detail by Johnston et al. (*35*). Briefly, duplicate peepers 1.5 m long (cell vertical spacing = 0.05 m) were installed along each transect and allowed to equilibrate for up to 38 days—effectively averaging any short-term dynamism in solute concentrations due to tidal fluctuations. After peeper retrieval, porewater redox potential (SHE) and pH were measured immediately using freshly calibrated electrodes. Aliquots of filtered (0.45 μm) porewater were analyzed for Fe^{2+} and total Fe using the 1,10-phenanthroline method (*30*) and HCO_3^- was determined according to Sarazin et al. (*36*). Remaining filtrate was preserved with HNO_3 and stored in the dark at 4 °C for subsequent analysis of total As by ICP-MS (Perkin-Elmer ELAN-DRCe), operated in DRC mode to optimize interference removal. Five percent of samples were analyzed in duplicate and had a precision within 6% (detection limit of 3.6 μg/L). Aqueous As speciation was determined by spectrophotometry (detection limit of 6.7 μg/L) on additional porewater samples (0.45 μm filtered) from Transect 1, that were collected by centrifugation of fresh sediment (*37*).

Results and Discussion

Tidally Influenced Hydrology. At both transects, the hydrology, redox potential, and pH was strongly influenced by tides. Former sulfuric horizons in the intertidal zone were regularly inundated (Figure 1, Figure SI2 of the Supporting Information). Tidal inundation frequency increased downslope and was accompanied by increasing soil moisture contents, declining Eh, and increasing pH in former sulfuric horizons (Table SI1 of the Supporting Information). The greatest variability in Eh occurred near the supratidal−intertidal fringe (Table SI1). At most sites, a thin oxic layer with lower pH values (<4.5) remained near the surface (Figure 1, Figure SI2).

Tidal inundation not only provides an overarching geochemical control, it also generates highly dynamic groundwater behavior at both transects (Figures SI3 and SI4 of the Supporting Information). The former sulfuric horizons at this site are highly transmissive, with hydraulic conductivities ranging from 4.98×10^{-5} to 1.78×10^{-3} m s^{-1}, which allows rapid propagation of the tidal signal. The resultant tidal forcing generates oscillating horizontal hydraulic gradients (Figures SI3 and SI4 of the Supporting Information), consistent with other studies of fringing intertidal sediments (*23, 24*). During the ebb-tide phase, the development of seaward hydraulic gradients promotes upward advection and seepage of porewaters along the intertidal slope. It has been demonstrated that such behavior can generate substantial solute flux from underlying groundwater to overlying surface waters, particularly in sediments with high hydraulic conductivity (*23, 24*).

General Soil Properties. Solid phase Fe(II) increased downslope as a proportion of reactive Fe (Table SI1 of the Supporting Information). This is indicative of Fe(III) reduction and reflects the hydro-redox gradient established by seawater inundation. Reactive Fe also increased near the soil surface in the intertidal zone (Figure 1, Figure SI2 of the Supporting Information). TOC contents were up to 8% near the surface and decreased to around 2% at depth (Figure SI2).

In accord with the findings of Johnston et al. (*21*), pyrite is reforming within former sulfuric horizons in the low elevation sections of both transects (Transect 1 at 100 m; Transect 2 at 80 and 100 m). This is consistent with their lower redox status and longer period of seawater inundation. Evidence of sulfate reduction in former sulfuric horizons includes elevated molar $Cl:SO_4$ ratios (~40, seawater = 19.6) and a downslope increase in their S_{CR} contents (Figure 1, Figure SI2).

Solid-Phase As. Total As (As_{Tot}) concentrations in soils were up to 40 μg/g (Figure 1, Figure SI2 of the Supporting Information), with mean concentrations of 15−21 μg/g at Transects 1 and 2, respectively (Table 1). There was a strong positive relationship between As_{Tot} and reactive Fe ($r^2 = 0.64$, α 0.01) in former sulfuric horizons, whereas there was no such relationship apparent in underlying sulfidic sediments (Figure SI5 of the Supporting Information). In contrast, sulfidic sediments displayed a positive relationship between As_{Tot} and pyrite-Fe ($r^2 = 0.37$, α 0.05, Figure SI5). Such different relationships are consistent with the contrasting pedogenesis of these materials and the hypothesized role of reactive Fe and pyrite as preferential carrier phases for As.

There was distinct enrichment of As within key Fe mineral phases. Jarosite (Figure SI6 of the Supporting Information)

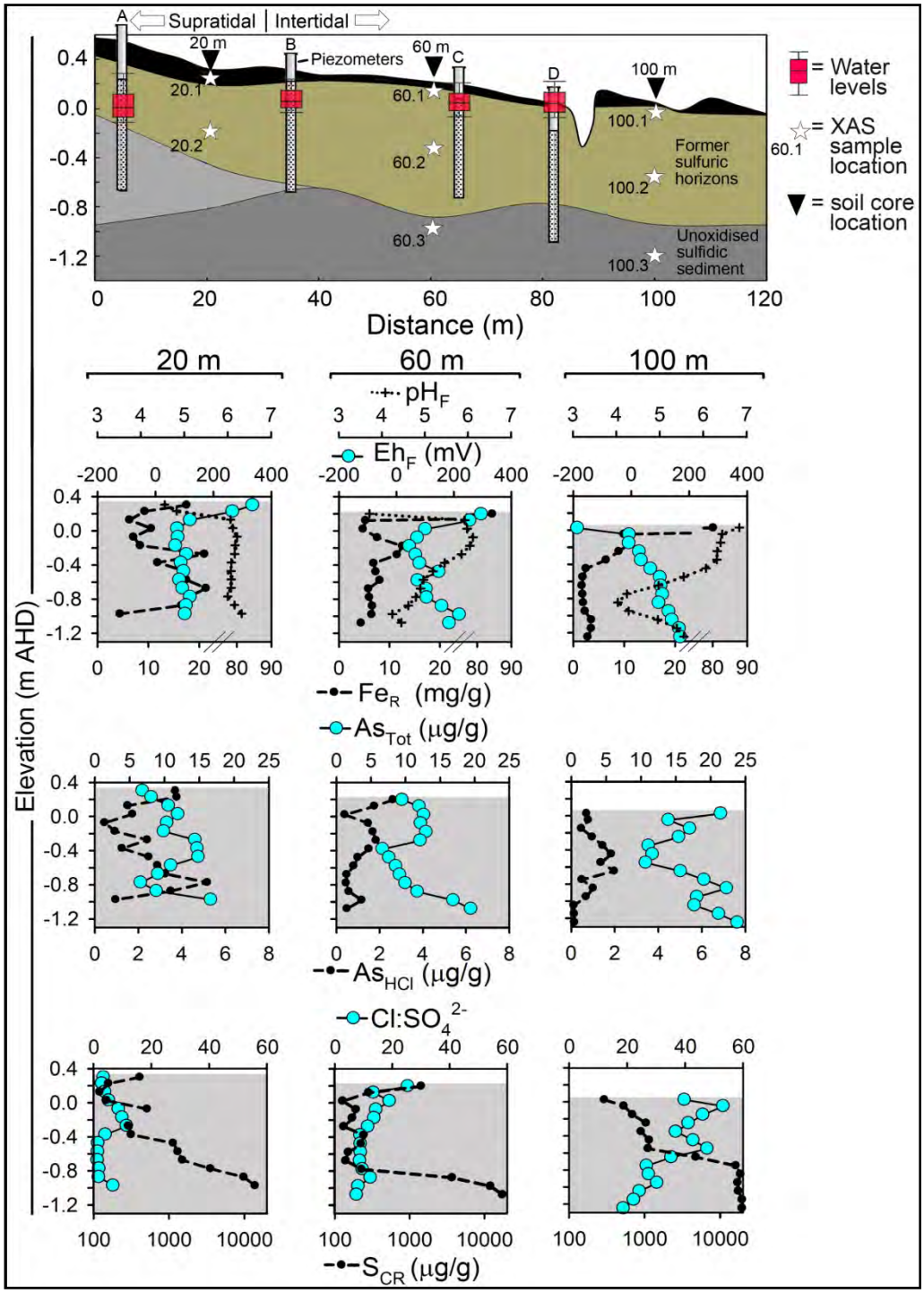

FIGURE 1. Transect 1 stratigraphy, hydrology, solid-phase characteristics, and the location of soil samples subject to X-ray absorption spectroscopy (XAS). Groundwater levels in piezometers A–D are from November 2007 to November 2008. Piezometer depth and slotting zones are drawn to vertical scale.

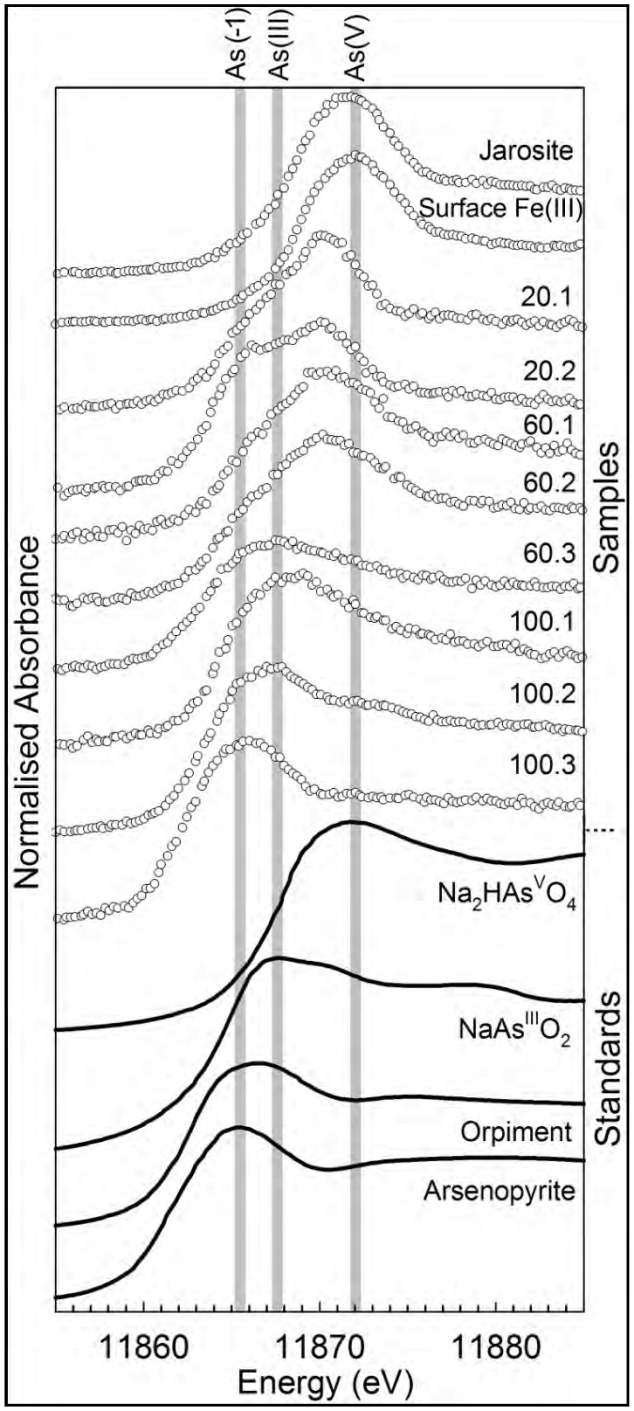

FIGURE 2. Arsenic K-edge XANES spectra of jarosite, surface Fe(III)-rich accumulation, and soil samples in comparison to several As standards (shown as solid lines). Soil sample locations are shown in Figure 1.

TABLE 1. Mean (± Standard Deviation) Concentrations of Solid-Phase Arsenic within Transect Soils and Fractions Rich in Fe Minerals

location/soil fraction (*n*)	near-total extract[a] (μg/g)
Transect 1 (55)	15.3 ± 4.0
Transect 2 (65)	20.9 ± 7.1
matrix[b] (4)	13.1 ± 4.6
jarosite[c] (4)	75.7 ± 14.7
surface Fe(III)-rich accumulations[d] (34)	36.1 ± 26.3
pyrite[e] (2)	279.0 ± 24.9

[a] Aqua-regia digest, except for pyrite. [b] Soil matrix surrounding jarosite pedofeatures. [c] Jarosite soil pedofeatures collected from former sulfuric horizons at Transects 1 and 2. [d] Collected from 0−0.01 m depth bgl. [e] Heavy-liquid extracted fraction, concentrated HNO_3 digest according to Huerta-Diaz et al. (*33*). Based on Fe content, this extract contained approximately 51% pyrite by mass.

was enriched by a factor of ~4−5 (75 μg/g) compared to immediately surrounding soil matrix (Table 1), which is of a similar order to that reported by Dudas (*12*). The sulfidic sediment derived dense mineral fraction (comprised mainly of pyrite and some marcasite; Figure SI6), was enriched in As by more than an order of magnitude compared to bulk soils (Table 1). In addition, surface Fe-rich accumulations (0−0.01 m; 5 to 40% Fe w/w, Figure SI7 of the Supporting Information) also had elevated As contents (1−6×) (Table 1), with As_{Tot} positively correlated ($r^2 = 0.34$, α 0.05) with Fe_R (Figure SI7). These surface accumulations had abundant Fe(III) (mean 81 ± 14% of Fe_{HCl}) and contained a variety of Fe(III) minerals including schwertmannite, lepidocrocite, goethite, and ferrihydrite (*22*).

Arsenic K-edge XANES analysis revealed distinct down-profile and downslope trends in solid-phase As speciation, consistent with the seawater-induced redox gradient. The XANES spectrum of the unoxidised sulfidic sediment at 100 m indicates that an FeAsS-like phase was an important reservoir for As in the original, undrained parent material. Solid-phase As in both jarosite and surficial Fe(III)-rich material was mainly As(V) (Figure 2). Near the surface and within former sulfuric horizons at 20 and 60 m (Transect 1), the XANES data revealed a mixture of As(V) and As(III) (Figure 2). In contrast, the XANES spectra for samples from the surface and in the former sulfuric horizon at 100 m, display edge positions consistent with As(III) or As sulfides (Figure 2). Overall, the XANES data demonstrate that seawater inundation of CASS is leading to reduction of solid-phase As(V) to As(III) and, subsequently, to reformation of As sulfides within former sulfuric horizons.

Porewater Geochemistry. Porewater salinity increased downslope while the redox potential generally declined (Figure SI8 of the Supporting Information). There was a distinct zone of As mobilization in porewaters at both transects, where concentrations exceeded 400 μg/L (Figure 3, Figure SI8). The zone of maximum porewater As was spatially associated with former sulfuric horizons near the intertidal limit. Speciation data suggests that most of this aqueous As (~80%) was As(III) (Table SI2 of the Supporting Information). This is consistent with XANES analysis and the important role of As(III) production in As release under reducing conditions (*4, 38*), plus the fact that As(III) is more readily desorbed from Fe(III) (hydr)oxides than As(V) (*4*). There were also very high concentrations of porewater Fe^{2+} (~2000 mg/L) in this same zone (Figure 3, Figure SI8), providing strong evidence for reductive dissolution of secondary Fe(III) minerals. Close coupling of arsenic and ferrous iron release has been demonstrated to occur during controlled reflooding of natural, iron-rich wetland sediments

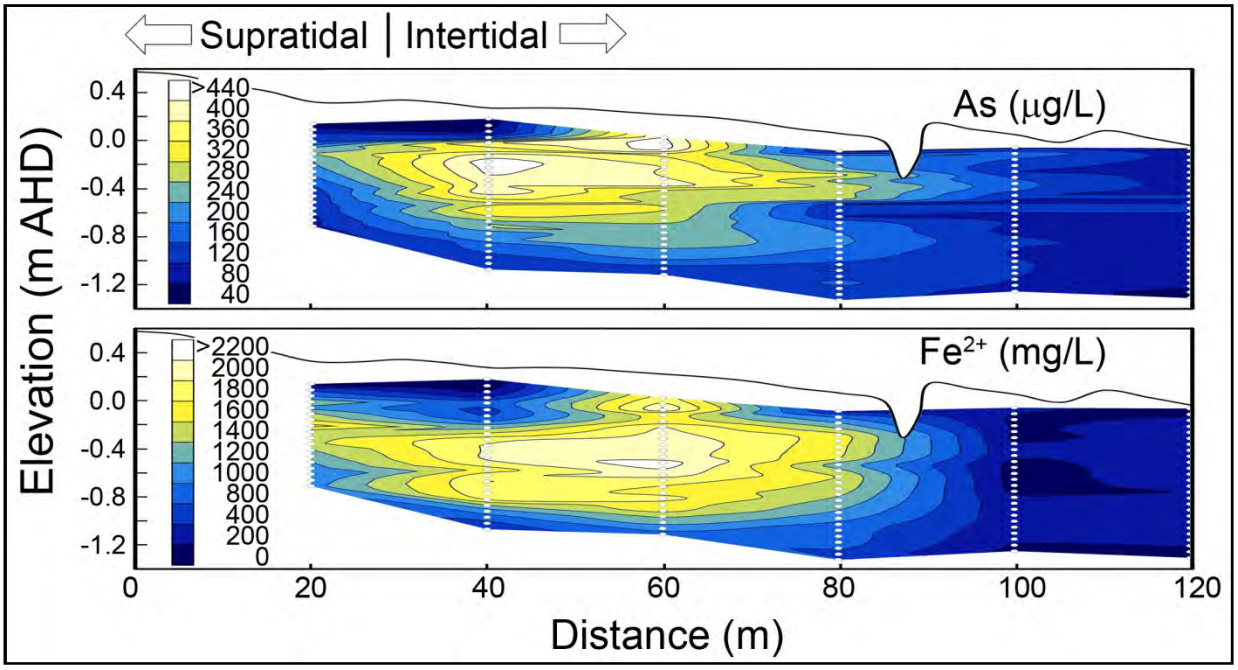

FIGURE 3. Porewater As and Fe^{2+} at Transect 1.

(*3, 39, 40*). There was a significant positive relationship between As and $Fe_{(aq)}^{2+}$ in the zone of mobilization (r^2 = 0.71, α 0.01, Figure 4). This is consistent with reductive dissolution of As-enriched Fe(III) minerals being a key process responsible for As mobilization (*2, 4*). There was also a strong positive correlation between As and HCO_3^- at the same locations (r^2 = 0.63, α 0.01, Figure 4). Bicarbonate competes with As for adsorption sites (*1*), and this may be an additional mechanism responsible for elevated porewater As. Anaerobic carbon metabolism via Fe reduction also generates HCO_3^-, and hence, there is potential for coupling of both processes.

Porewater As concentrations were lower above the intertidal limit. Porewater As also decreased toward the lower sections of both transects in the zone of contemporary pyrite reformation. Dissolved As can be effectively sequestered by iron-sulfide minerals through surface complexation, which is more effective as pH increases (*7*), and coprecipitation (*6*). Both are probable mechanisms of attenuation, not only for As, but also Fe^{2+}. This spatial pattern of As mobilization is consistent with the work of Burton et al. (*3*) and Root et al. (*6*) who found that As release was greatest in the transition between iron-oxidized and sulfate-reducing conditions.

Tidal Pumping: A Mechanism for Redistribution and Surface Accumulation. The coupling of a redox transition triggering As mobilization with physical forcing processes is an important feature of seawater inundation of CASS. The shallow fringing aquifer's former sulfuric horizons have effectively been transformed into a subterranean estuary with oscillating hydraulic gradients that create potential for dynamic exchange of aqueous species with overlying surface waters (*23, 24*). On multiple occasions, the authors observed visual evidence of groundwater seepage via surface-connected pores along the intertidal slope during the ebb-tide. To explore this further, changes in surface water chemistry were monitored at 60 m at Transect 1 during a single tidal cycle (described in detail in the Supporting Information). During the ebb-tide phase, negative (upward) vertical hydraulic gradients were associated with large changes in the geochemistry of overlying tidal surface waters (Figure 5). There was a three order increase in the concentration of Fe^{2+} (>300 mg/L), increasing As (>30 μg/L) plus declining pH and Cl^-:SO_4^{2-} ratios in the overlying surface waters, reflecting an upward porewater flux from underlying former sulfuric horizons.

Such upward advection of As- and Fe^{2+}-rich porewater followed by Fe oxidation and precipitation, readily explains the observed surficial accumulation of material rich in both reactive Fe(III) and As (Figure SI7 of the Supporting Information). From one perspective, this process could be regarded as forming a natural, reactive-Fe barrier, similar to that described by Bone et al. (*5*), except that the reactive-Fe is accumulating at the sediment−surface water interface rather than at depth. While this material may retard the flux of porewater As to overlying waters, this data demonstrates that in some instances it is not completely effective. In addition, the Fe(III) minerals formed are prone to reductive

Cite as: Johnston S.G., Keene A.F., Burton E.D., Bush R.T., Sullivan L.A., McElnea A.E., Ahern C.R., Smith C.D., Powell B. (2010) Arsenic mobilisation in a seawater inundated acid sulfate soil. *Environmental Science and Technology* 44 (6), 1968–1973

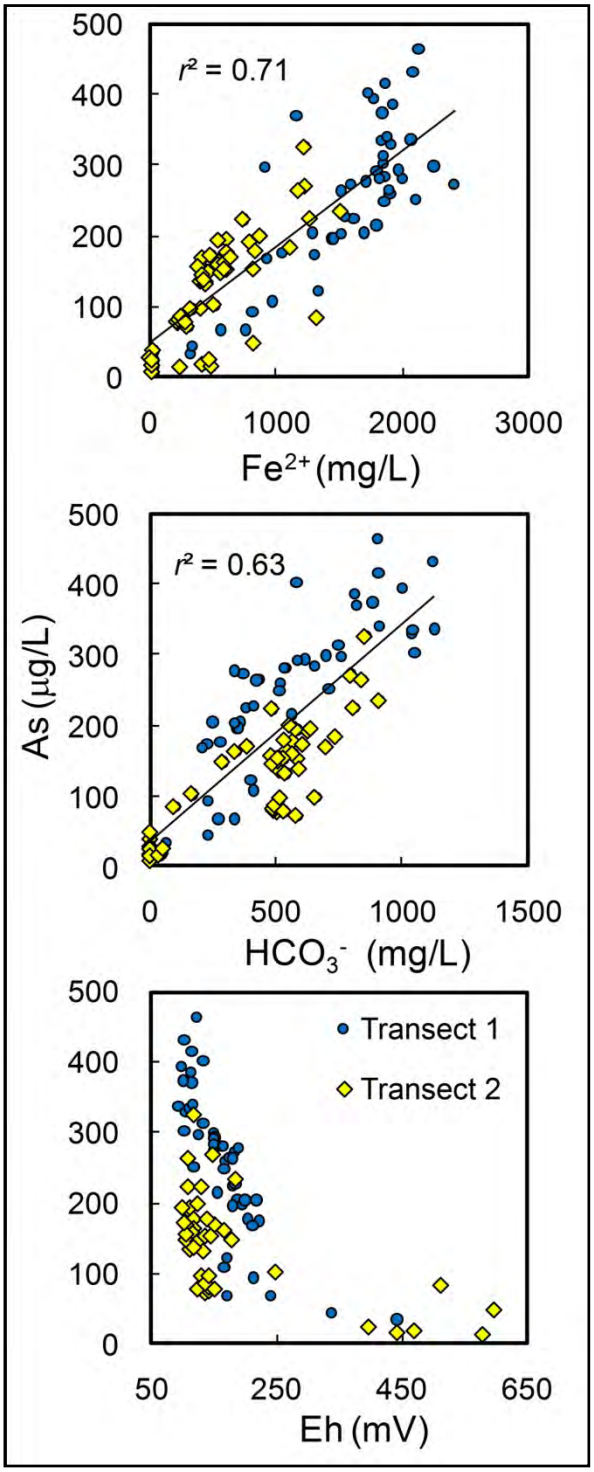

FIGURE 4. Relationships between porewater As and Fe^{2+}, HCO_3^-, and redox potential (SHE) from Transect 1 and 2 at a 60 m distance.

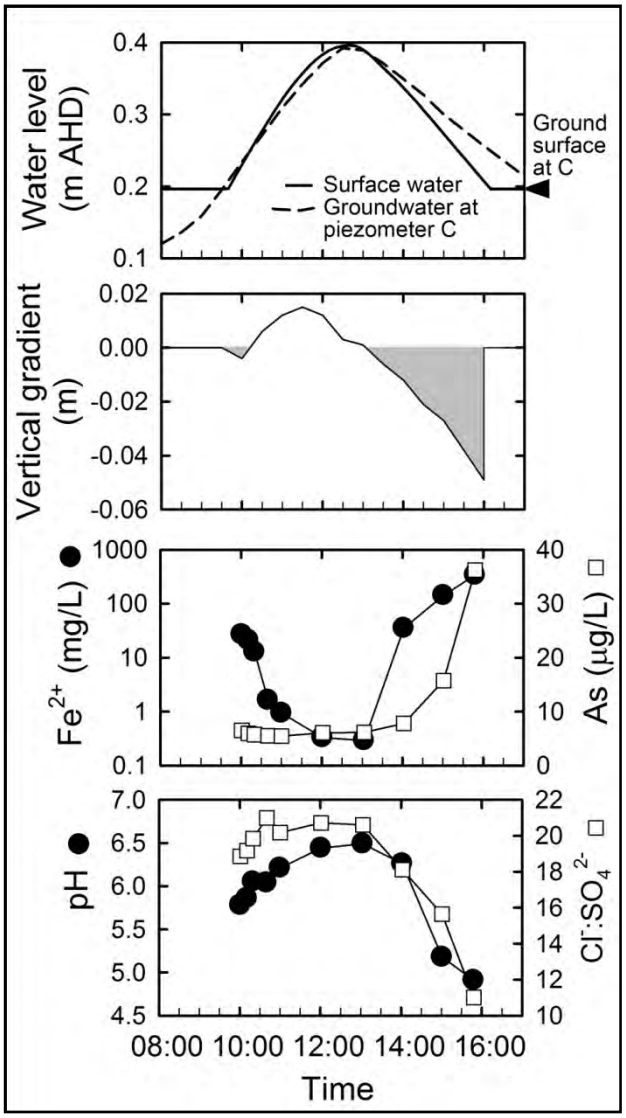

FIGURE 5. Tidal cycle changes in groundwater and surface water levels (Transect 1, piezometer C) and corresponding vertical head gradients in relation to overtopping surface water Fe^{2+}, As, pH, and $Cl^-:SO_4^{2-}$ ratios (molar). Periods favoring upwelling (negative hydraulic gradients) are shaded gray.

dissolution if redox boundaries migrate upward and may thereby influence future water quality.

Zones of As Mobilization, Attenuation, and Accumulation. Seawater inundation of a CASS toposequence has caused a major shift in the solid and aqueous phase speciation, distribution, and partitioning of As. While there is evidence of considerable As mobilization, it appears to be spatially localized between two distinct geochemical regimes. Distinct hydro-geochemical zonation is evident across the seawater inundation fringe where As geochemistry is intimately bound with the fate and behavior of Fe and S. Our results are synthesized in a conceptual model which represents this hydro-geochemical zonation (Figure 6).

According to this model, oxidation of As-rich pyrite in the drained sulfidic parent material led to (*1*) the formation of acid sulfate conditions with preferential enrichment of As(V) in secondary Fe(III) minerals (e.g., jarosite). Seawater inundation (*2*) initiates reducing conditions stimulating As mobilization by several processes including (a) reductive dissolution of As-bearing secondary Fe(III) minerals, (b) reduction of As(V) to As(III), and (c) competitive anion desorption by HCO_3^-. Tidal pumping facilitates upward advection (*3*) of Fe^{2+}- and As(III)-rich porewaters in the intertidal zone, where subsequent oxidation in surficial sediments results in the accumulation of tertiary Fe(III)-minerals enriched in As(V). Further downslope (*4*) there is attenuation of porewater As in the zone of contemporary pyrite reformation, where solid phase As occurs predominantly in the form of As(III).

The findings of this study have geochemical relevance to sea-level rise induced redox cycling of As in Fe-rich coastal floodplain aquifers. They clearly demonstrate there is considerable potential for As mobilization during seawater inundation of CASS. To manage this environmental hazard, it may be important to minimize drainage from the shallow fringing aquifer during the period of redox transition while As is mobile. The accumulation of As within redox-sensitive surficial sediments may have longer term consequences for water quality and is worthy of further investigation.

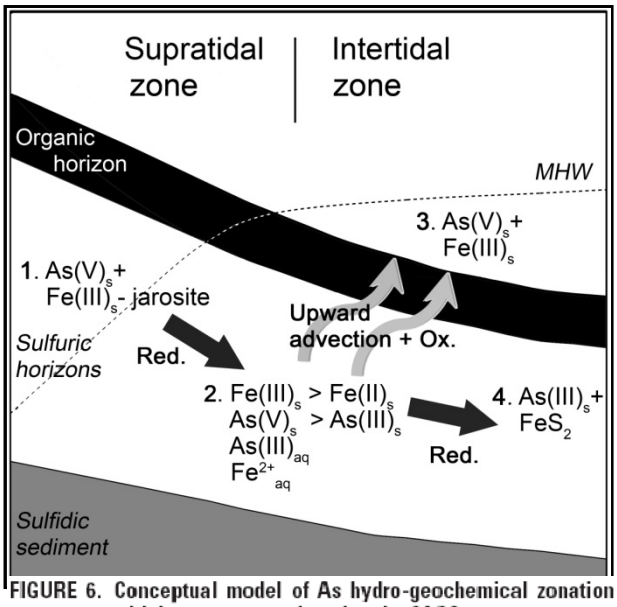

FIGURE 6. Conceptual model of As hydro-geochemical zonation across a tidal, seawater inundated CASS toposequence. Numbers 1−4 represent important As and Fe species and their proximate spatial occurrence. Black arrows represent the progressive geochemical trajectory of reductive transformations following seawater inundation. Gray arrows represent upward advection of aqueous As(III) and Fe^{2+} in the intertidal zone plus oxidation and accumulation at the surface. MHW is mean high water.

Acknowledgments

We thank Michelle Bush for XRD analysis and DERM field staff for their assistance. This project was funded by the Cooperative Research Centre for Contamination Assessment and Remediation of the Environment (6-6-01-06/07 "A National Demonstration Site for Innovative Acid Sulfate Soil Management") and the Queensland Department of Environment and Resource Management. The XANES work was funded by the Australian Synchrotron Research Program (AS083/ANBF711), and we thank Bernd Johannesson and Garry Foran for assistance at the Australian National Beamline Facility, Tsukuba, Japan. R.T.B. and E.D.B. were supported by Australian Research Council fellowships. Thanks to three anonymous referees for their constructive comments.

Supporting Information Available

Location map, Transect 2 stratigraphy, hydrology and solid-phase characteristics, time-series groundwater levels, solid-phase As and Fe fraction relationships, X-ray diffractograms, As content of surficial (0−0.01 m) Fe-rich accumulations, Transect 2 porewater geochemistry, tidal cycle surface water chemistry, mean solid-phase properties, and aqueous As speciation. This material is available free of charge via the Internet at http://pubs.acs.org.

Literature Cited

(1) Smedley, P. L.; Kinniburgh, D. G. A review of the source, behaviour and distribution of arsenic in natural waters. *Appl. Geochem.* **2002**, *17*, 517–568.

(2) Polizzotto, M. L.; Kocar, B. D.; Benner, S. G.; Sampson, M.; Fendorf, S. Near-surface wetland sediments as a source of arsenic release to ground water in Asia. *Nature* **2008**, *454*, 505–508.

(3) Burton, E. D.; Bush, R. T.; Sullivan, L. A.; Johnston, S. G.; Hocking, R. K. Mobility of arsenic and selected metals during re-flooding of iron- and organic-rich acid-sulfate soil. *Chem. Geol.* **2008**, *253*, 64–73.

(4) Tufano, K. J.; Reyes, C.; Saltikov, C. W.; Fendorf, S. Reductive processes controlling arsenic retention: revealing the relative importance of iron and arsenic reduction. *Environ. Sci. Technol.* **2008**, *42*, 8283–8289.

(5) Bone, S. E.; Gonneea, M. A.; Charette, M. A. Geochemical cycling of arsenic in a coastal aquifer. *Environ. Sci. Technol.* **2006**, *40*, 3273–3278.

(6) Root, R. A.; Vlassopoulos, D.; Rivera, N. A.; Rafferty, M. T.; Andrews, C.; O'Day, P. A. Speciation and natural attenuation of arsenic and iron in a tidally influenced shallow aquifer. *Geochim. Cosmochim. Acta* **2009**, *73*, 5528–5553.

(7) Bostick, B. C.; Chen, C.; Fendorf, S. Arsenite retention mechanisms within estuarine sediments of Pescadero, CA. *Environ. Sci. Technol.* **2004**, *38*, 3299–3304.

(8) Jung, H. B.; Charette, M. A.; Zheng, Y. Field, laboratory, and modeling study of reactive transport of groundwater arsenic in a coastal aquifer. *Environ. Sci. Technol.* **2009**, *43*, 5333–5338.

(9) Andriesse, W.; van Mensvoort, M. E. F. Acid Sulfate Soils: Distribution and Extent. In *Encyclopedia of Soil Science: Volume 1*, second ed.; Rattan, L., Ed.; CRC Press: Boca Raton, FL, 2006; pp 14−19.

(10) Sullivan, L. A.; Bush, R. T. Iron-precipitate accumulations associated with waterways in drained coastal acid sulfate soil landscapes of eastern Australia. *Marine Freshwater Res.* **2004**, *55*, 727–736.

(11) Burton, E. D.; Bush, R. T.; Johnston, S. G.; Watling, K.; Hocking, R. K.; Sullivan, L. A.; Heber, G. K. Sorption of arsenic(V) and arsenic(III) to schwertmannite. *Environ. Sci. Technol.* **2009**, *43*, 9202–9207.

(12) Dudas, M. J. Enriched Levels of Arsenic in Post-Active Acid Sulfate Soils in Alberta. *Soil Sci. Soc. Am. J.* **1984**, *48*, 1451–1452.

(13) Carlson, L.; Bigham, J. M.; Schwertmann, U.; Kyek, A.; Wagner, F. Scavenging of As from acid mine drainage by schwertmannite and ferrihydrite: A comparison with synthetic analogues. *Environ. Sci. Technol.* **2002**, *36*, 1712–1719.

(14) Fukushi, K.; Sasaki, M.; Sato, T.; Yanasa, N.; Amano, H.; Ikeda, H. A natural attenuation of arsenic in drainage from an abandoned arsenic mine dump. *Appl. Geochem.* **2003**, *18*, 1267–1278.

(15) Savage, K. S.; Bird, D. K.; O'Day, P. A. Arsenic speciation in synthetic jarosite. *Chem. Geol.* **2005**, *215*, 473–498.
(16) Appleyard, S.; Wong, S.; Willis-Jones, B.; Angeloni, J.; Watkins, R. Groundwater acidification caused by urban development in Perth, Western Australia: source, distribution, and implications for management. *Aust. J. Soil Res.* **2004**, *42*, 579–585.
(17) Appleyard, S. J.; Angeloni, J.; Watkins, R. Arsenic-rich groundwater in an urban area experiencing drought and increasing population density, Perth, Australia. *Appl. Geochem.* **2006**, *21*, 83–97.
(18) Nguyen, K. P.; Ryuichi, I. Source and release mechanism of arsenic in aquifers of the Mekong Delta, Vietnam. *J. Contaminant. Hydrol.* **2009**, *103*, 58–69.
(19) van Breemen, N.; Harmsen, K. Translocation of iron in acid sulfate soils: I. Soil morphology and mineralogy of iron in a chronosequence of acid sulfate soils. *Soil Sci. Soc. Am. J.* **1975**, *39*, 1140–1148.
(20) Powell, B.; Martens, M. A review of acid sulfate soil impacts, actions and policies that impact on water quality in the Great Barrier Reef catchments, including a case study on remediation at East Trinity. *Mar. Pollut. Bull.* **2005**, *51*, 149–164.
(21) Johnston, S. G.; Keene, A. F.; Bush, R. T.; Burton, E. D.; Sullivan, L. A.; Smith, D.; Martens, M. A.; McElnea, A. E.; Wilbraham, S. T.; van Heel, S. Contemporary pedogenesis of severely degraded tropical acid sulfate soils after introduction of regular tidal inundation. *Geoderma* **2009**, *149*, 335–346.
(22) Johnston, S. G.; Burton, E. D.; Bush, R. T.; Keene, A. F.; Sullivan, L. A.; Smith, D.; McElnea, A. E.; Ahern, C. R.; Powell, B. Abundance and fractionation of Al, Fe and trace metals following tidal inundation of a tropical acid sulfate soil. *Appl. Geochem.* **2010**, *25*, 323–335.
(23) Wilson, A. M.; Gardner, L. R. Tidally driven groundwater flow and solute exchange in a marsh: Numerical simulations. *Wat. Resour. Res.* **2006**, *42*, W01405.
(24) Robinson, C.; Li, L.; Barry, D. A. Effect of tidal forcing on a subterranean estuary. *Adv. Water Res.* **2007**, *30*, 851–865.
(25) Solomon, S., Qin, D., Manning, M., Chen, Z., Marquis, M., Averyt, K. B., Tignor, M., Miller, H. L., Eds. *Climate Change 2007: The Physical Science Basis. Contribution of Working Group I to the Fourth Assessment Report of the Intergovernmental Panel on Climate Change*; Cambridge University Press: Cambridge, United Kingdom, and New York, 2007.
(26) Cook, F. J.; Hicks, W.; Gardner, E. A.; Carlin, G. D.; Froggatt, D. W. Export of acidity in drainage water from acid sulfate soils. *Marine Pollut. Bull.* **2000**, *41*, 319–326.
(27) Johnston, S. G.; Bush, R. T.; Sullivan, L. A.; Burton, E. D.; Smith, D.; Martens, M. A.; McElnea, A. E.; Ahern, C. R.; Powell, B.; Stephens, L. P.; Wilbraham, S. T.; van Heel, S. Changes in water quality following tidal inundation of coastal lowland acid sulfate soil landscapes. *Estuarine, Coast. Shelf Sci.* **2009**, *81*, 257–266.
(28) Kostka, J. E.; Luther, G. W. Partitioning and speciation of solid phase Fe in saltmarsh sediments. *Geochim. Cosmochim. Acta* **1994**, *58*, 1701–1710.
(29) Wallmann, K.; Hennies, K.; König, I.; Petersen, W.; Knauth, H. D. New procedure for determining reactive Fe(III) and Fe(II) minerals in sediments. *Limnol. Oceanogr.* **1993**, *38*, 1803–1812.
(30) *Standard methods for the examination of water and wastewater*; American Public Health Association - American Water Works Association; Baltimore, MD, 2005.
(31) Raiswell, R.; Canfield, D. E.; Berner, R. A. A comparison of iron extraction methods for the determination of degree of pyritisation and the recognition of iron-limited pyrite formation. *Chem. Geol.* **1994**, *111*, 101–110.
(32) Sullivan, L. A.; Bush, R. T.; McConchie, D. M. A modified chromium reducible sulfur method for reduced inorganic sulfur: optimum reaction time for acid sulfate soil. *Aust. J. Soil Res.* **2000**, *38*, 729–734.
(33) Huerta-Diaz, M. A.; Carignan, R.; Tessier, A. Measurement of trace metals associated with acid volatile sulfides and pyrite in organic freshwater sediments. *Environ. Sci. Technol.* **1993**, *27*, 2367–2372.
(34) Tenderholt, A.; Hedman, B.; Hodgson, K. O. PySpline: A modern, cross-platform program for the processing of raw averaged XAS edge and EXAFS data. *AIP Conf. Proc.* **2006**, *882*, 105–107.
(35) Johnston, S. G.; Burton, E. D.; Keene, A. F.; Bush, R. T.; Sullivan, L. A.; Isaacson, L. Porewater sampling in acid sulfate soils: a new peeper method. *J. Environ. Qual.* **2009**, *38*, 2474–2477.
(36) Sarazin, G.; Michard, G.; Prevot, F. A rapid and accurate spectroscopic method for alkalinity measurements in sea water samples. *Water Res.* **1999**, *33*, 290–294.
(37) Dhar, R. K.; Zheng, Y.; Rubenstone, J.; van Geen, A. A rapid colorimetric method of measuring arsenic concentrations in groundwater. *Anal. Chim. Acta* **2004**, *526*, 203–209.
(38) Kocar, B. D.; Herbel, M. J.; Tufano, K. J.; Fendorf, S. Contrasting effects of dissimilatory iron(III) and arsenic(V) reduction on arsenic retention and transport. *Environ. Sci. Technol.* **2009**, *40*, 6715–6721.
(39) Blodau, C.; Fulda, B.; Bauer, M.; Knorr, K.-H. Arsenic speciation and turnover in intact organic soil mesocosms during experimental drought and rewetting. *Geochim. Cosmochim. Acta* **2008**, *72*, 3991–4007.
(40) Weber, F.-A.; Hofacker, A.; Voegelin, A.; Kretzschmar, R. Temperature dependence and coupling of iron and arsenic reduction and release during flooding of a contaminated soil. *Environ. Sci. Technol.* **2010**, *44*, 116–122.

SUPPORTING INFORMATION

Arsenic mobilization in a seawater inundated acid sulfate soil

Scott G. Johnston[A]*, Annabelle F. Keene[A], Edward D. Burton[A], Richard T. Bush[A], Leigh A. Sullivan[A], Angus E. McElnea[B], Col R. Ahern[B], C. Douglas Smith[B], Bernard Powell[B], Rosalie K. Hocking[C]

*Corresponding author (Scott G Johnston: scott.johnston@scu.edu.au)

[A]Southern Cross GeoScience
Southern Cross University, Lismore, NSW 2480, Australia

[B]Department of Environment and Resource Management, 80 Meiers Road, Indooroopilly, Qld. 4068, Australia

[C]Monash Centre for Synchrotron Science and School of Chemistry
Monash University, Clayton, Vic. 3800, Australia.

Contents

Figure SI 1	Study site location map
Figure SI 2	Transect 2 stratigraphy, hydrology and solid-phase characteristics
Figure SI 3	Transect 1 time-series groundwater levels
Figure SI 4	Transect 2 time-series groundwater levels
Figure SI 5	Linear regression between solid-phase As_{Tot} and Fe fractions
Figure SI 6	X-ray diffractograms of As-enriched Fe mineral phases
Figure SI 7	Surficial (0–1 cm) accumulations enriched in reactive Fe and As
Figure SI 8	Porewater geochemistry at Transect 2
Text SI 1	Additional methods
Table SI 1	Sulfuric horizon mean solid-phase soil properties
Table SI 2	Aqueous As speciation at Transect 1

Cite as: Johnston S.G., Keene A.F., Burton E.D., Bush R.T., Sullivan L.A., McElnea A.E., Ahern C.R., Smith C.D., Powell B. (2010) Arsenic mobilisation in a seawater inundated acid sulfate soil. *Environmental Science and Technology* 44 (6), 1968–1973

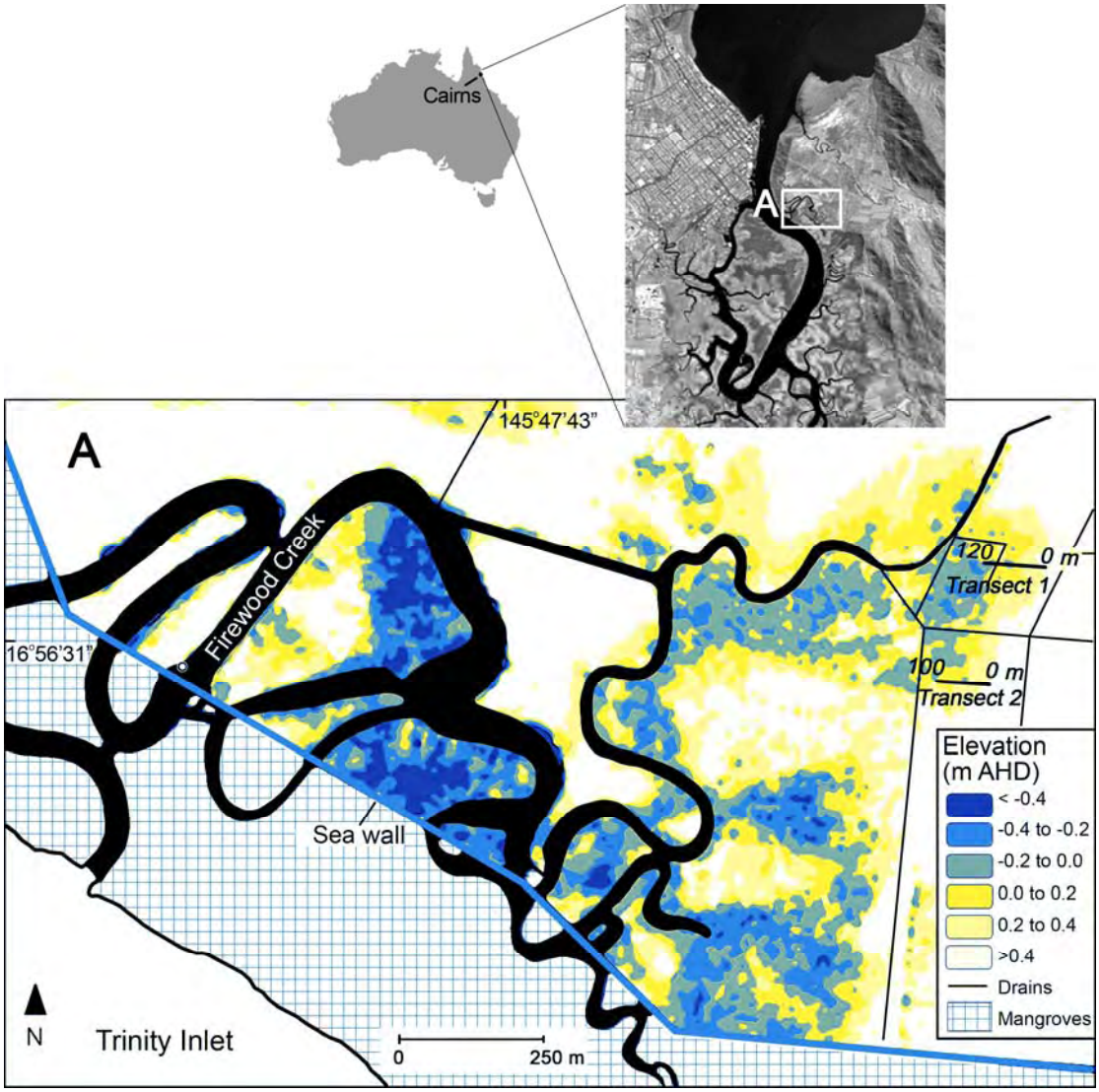

Figure SI 1. Location of study site, sea wall and transects, with surface elevation in Firewood Creek sub-catchment (Inset A). AHD is Australian Height Datum (0 m AHD ≈ mean sea level).

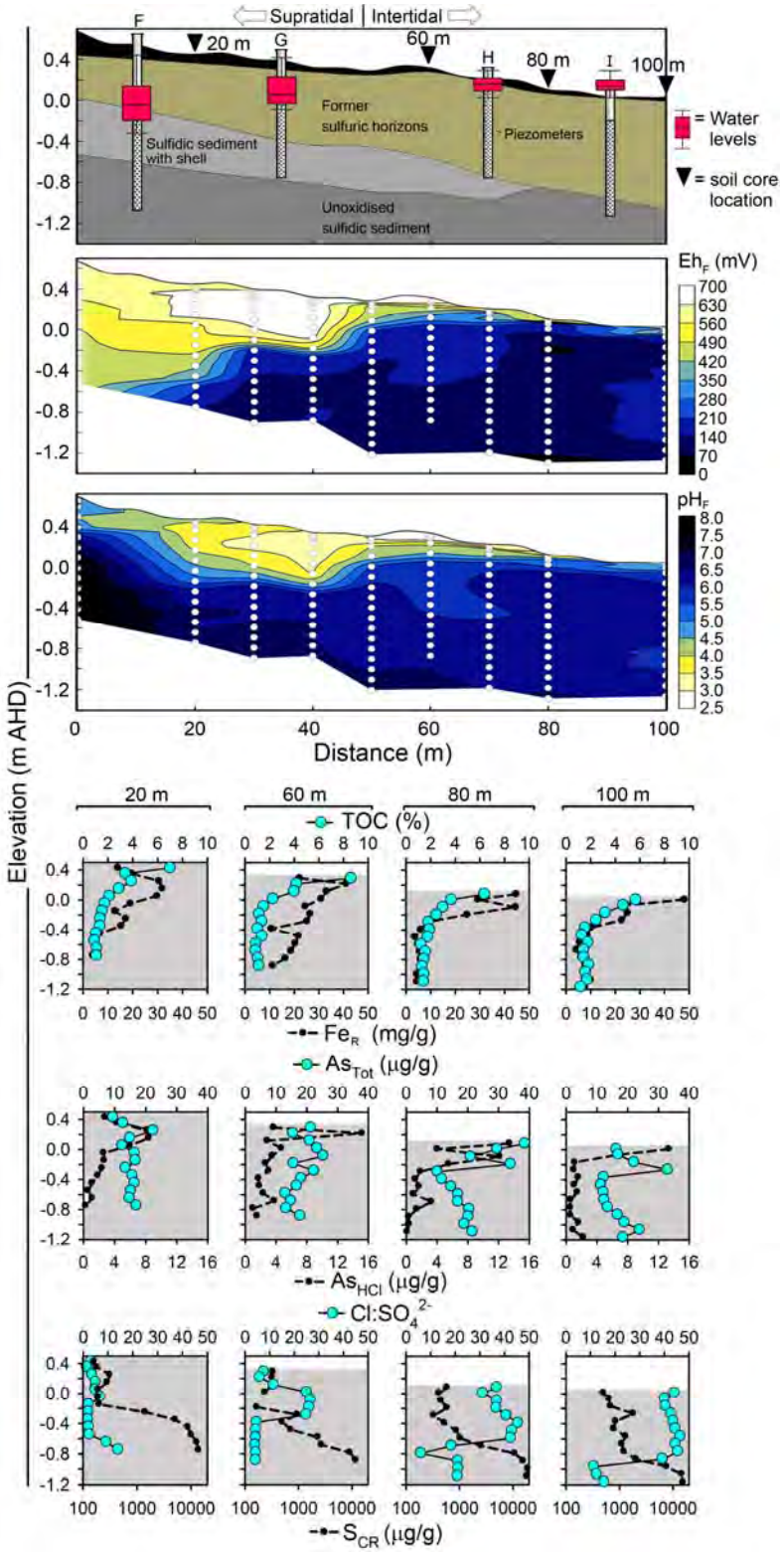

Figure SI 2. Transect 2 stratigraphy, hydrology and solid-phase characteristics. Groundwater levels in piezometers F-I are from November 2007 to November 2008. Piezometer depth and slotting zones are drawn to vertical scale.

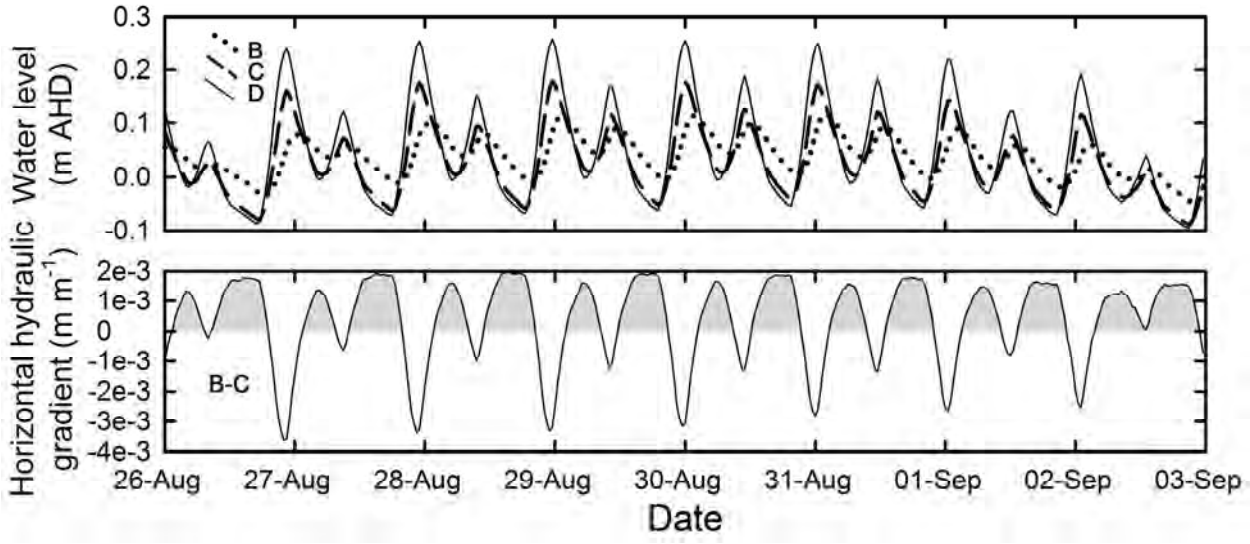

Figure SI 3. Transect 1 time-series groundwater levels (piezometers B, C, D) and corresponding horizontal hydraulic gradients between piezometers B-C. Periods of effluent (seaward) horizontal hydraulic gradients are shaded grey. Horizontal hydraulic gradients were calculated by dividing head difference by distance.

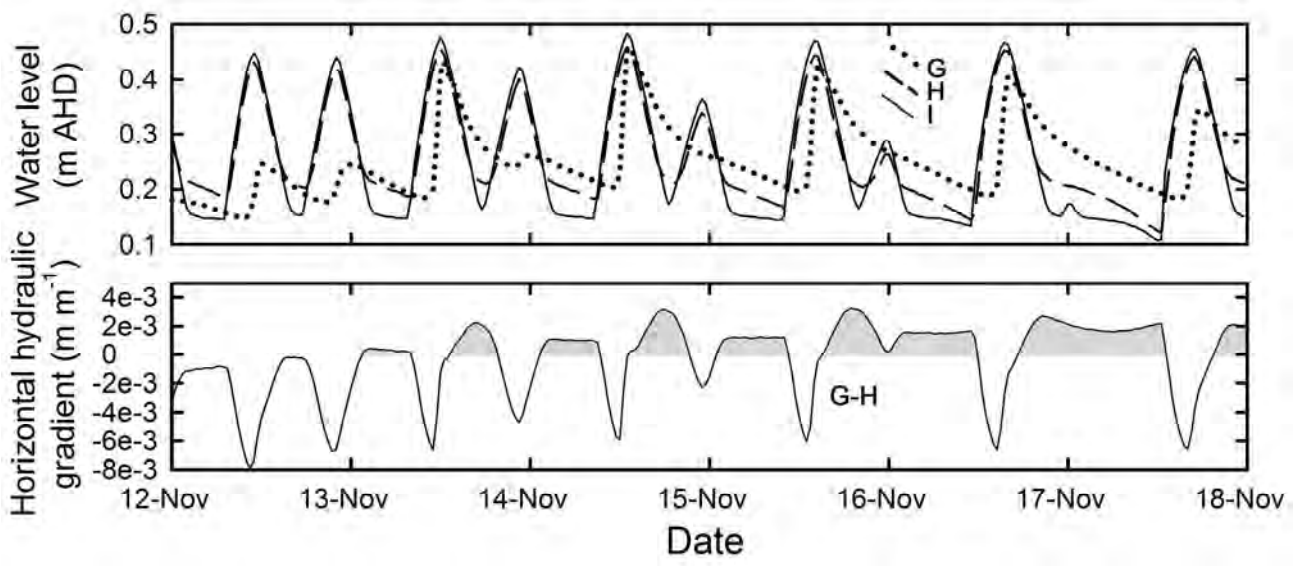

Figure SI 4. Transect 2 time-series groundwater levels (piezometers G, H, I) and corresponding horizontal hydraulic gradients between piezometers G-H. Periods of effluent (seaward) horizontal hydraulic gradients are shaded grey. Horizontal hydraulic gradients were calculated by dividing head difference by distance.

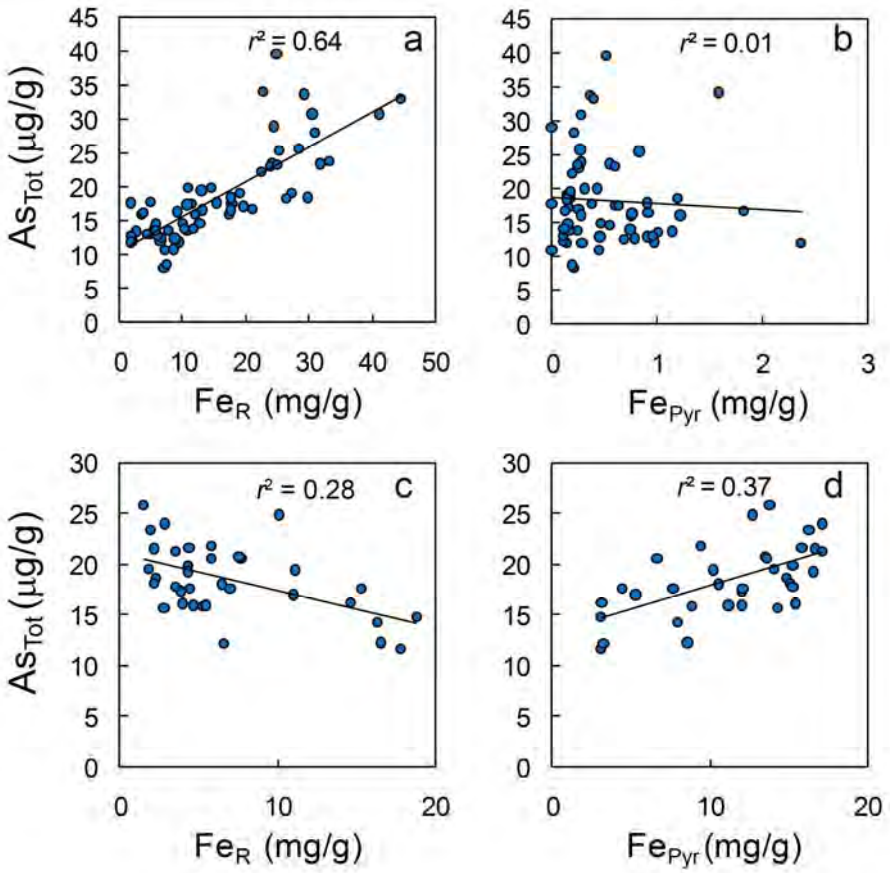

Figure SI 5. Linear regression between solid-phase near-total As [As_{Tot}] and reactive Fe [Fe_R] and Pyrite Fe (Fe_{Pyr}) in former sulfuric horizons (a), (b); and underlying sulfidic sediment (c), (d). Data points are from transect 1 and 2. Identification of former sulfuric horizons and sulfidic sediment is based on transect stratigraphy. Fe_{Pyr} is based on S_{CR} assuming a stoichiometric relationship between Fe:S of 1:2.

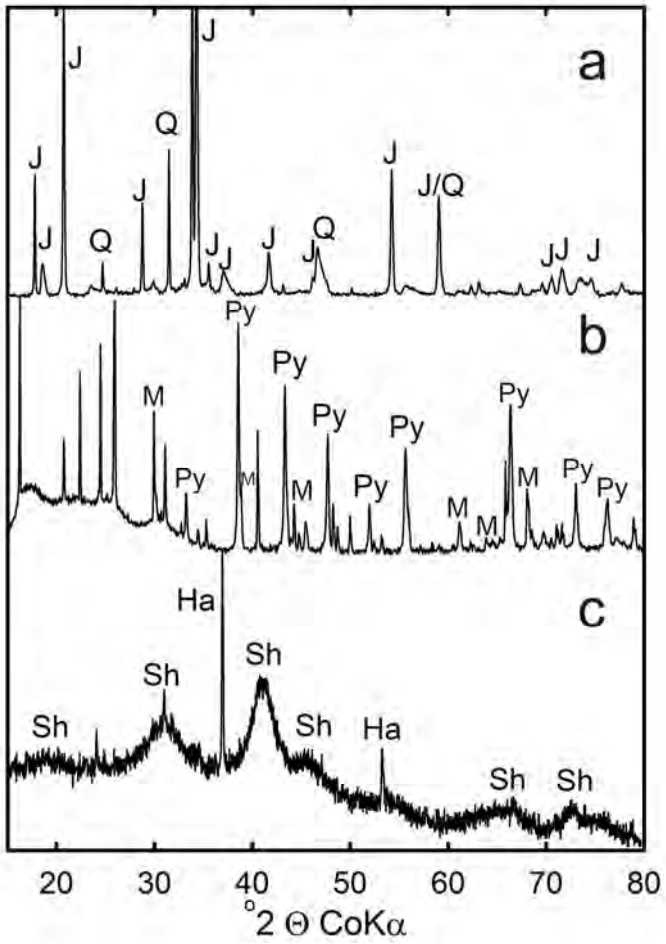

Figure SI 6. Representative X-ray diffractograms of As-enriched Fe mineral phases: (a) Jarosite pedofeature from former sulfuric horizon at Transect 1, (b) Pyritic heavy-liquid extracted fraction from unoxidized sulfidic sediment at Transect 1, 100 m (-1.0 to -1.2 m AHD), and (c) Schwertmannite dominant surficial (0–0.01 m) accumulation from Transect 2, 80 m. J, jarosite; Q, quartz; Py, pyrite; M, marcasite; Sh, schwertmannite; Ha, halite.

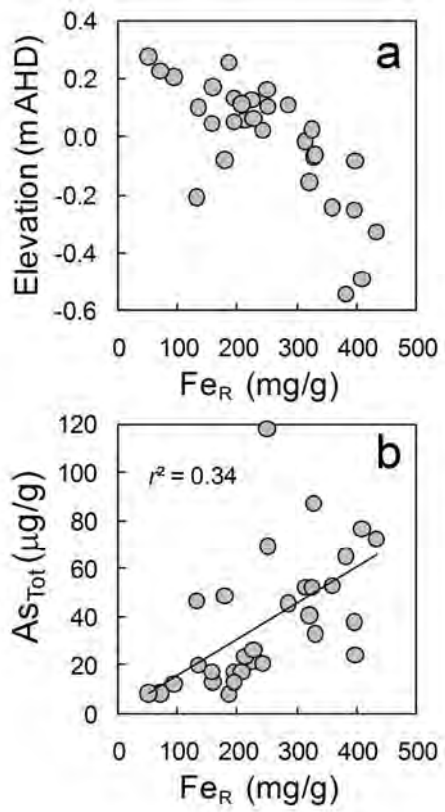

Figure SI 7. (a) Fe_R content of surficial (0–0.01 m) accumulations in relation to surface elevation, (b) relationship between Fe_R and As_{Tot} in surficial (0–0.01 m) Fe-rich accumulations.

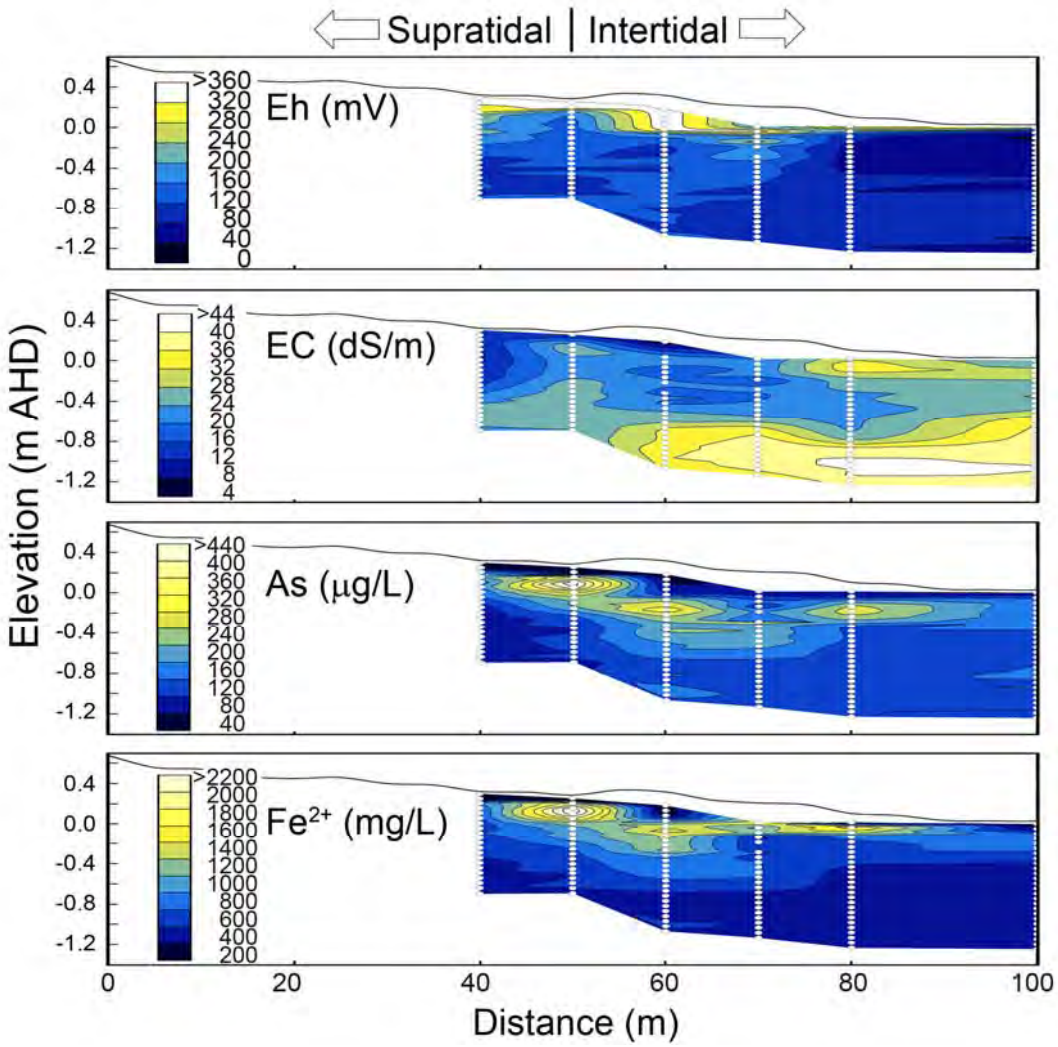

Figure SI 8. Porewater geochemistry at Transect 2.

Text SI 1

Additional methods

Hydrology

Groundwater levels were measured in 50 mm diameter PVC piezometers installed along each transect (5, 35, 65, 82 m at Transect 1; 10, 35, 68, 90 m Transect 2). Piezometers were up to 1.6 m below ground level and had screened intervals ranging from 0.8 to 1.2 m in length (depicted in correct vertical scale in Figure 1, Figure SI2). Groundwater levels were corrected to AHD using manual measurements from the top of each piezometer to the water table. Horizontal hydraulic gradients between adjacent piezometers were calculated by dividing head difference by distance. Vertical gradients were examined during a tidal cycle at Transect 1 and are the difference between groundwater levels and simultaneous measurements of overlying surface water levels in a stilling piezometer. The saturated hydraulic conductivity (K_s) of former sulfuric horizons was measured in duplicate at five locations along each transect via in situ recovery tests and auger-hole slug tests.

Solid-phase sampling and characterization

At each soil sampling location, field measurements of sediment pH (pH_F) and Eh (Eh_F) were made on duplicate cores immediately after core retrieval. Measurements were made by directly inserting an intermediate junction Ag/AgCl combination pH electrode (freshly calibrated using standard buffer solutions) and an intermediate junction Ag/AgCl combination platinum-tipped ORP electrode attached to a TPS 90-FLMV Field Lab meter until stable readings were obtained. Electrode redox potential was checked using a fresh ZoBell's solution and the KCl electrolyte of both electrodes replaced between sampling sites. All redox data presented here has been corrected to the standard hydrogen electrode. The method of direct probe insertion into soil inevitably results in the measurement of mixed redox potentials and does not account for the development of micro-scale redox heterogeneity. Soil samples were collected at 0–0.05 m, 0.05–0.15 m and in 0.1 m increments thereafter to a depth of 1.25 m below ground surface. Figures in this study display soil data using the mid-point of sampling depth increments.

Tidal cycle surface water quality monitoring

During a single flood-tide cycle, groundwater levels at piezometer C (Transect 1, 65 m) were recorded at 10 minute intervals using a submersible pressure transducer vented to the atmosphere (Odyssey, ODYPS05). Simultaneously, the overlying surface water levels were recorded manually in an immediately adjacent stilling piezometer. Vertical gradients are calculated by head difference. Surface water samples were collected within 5 m of piezometer C at regular intervals throughout the flood-tide cycle using a fixed, single-depth (0.02 m above sediment-water interface), Tygon tube connected to a 60 mL syringe sampling device. The syringe and tubing was flushed three times with sample water prior to collection and the sample immediately (within 2–5 minutes) filtered via a 0.45 · m syringe-driven filter. An aliquot was then preserved with HNO_3 and stored in the dark at 4 ^oC for later analysis

of total As by ICP-MS (Perkin-Elmer ELAN-DRCe), plus Cl and water soluble S by flow injection analysis (Lachat QuikChem 8000) and ICP-AES (Perkin-Elmer DV4300), respectively. Aliquots of filtrate were also preserved for determination of Fe^{2+} within 24 h of collection by the 1,10-phenanthroline method. pH was measured on a separate sub-sample using freshly a calibrated probe (intermediate junction Ag/AgCl).

Table SI1. Means (±standard deviation) of selected solid-phase properties in former sulfuric horizons (0–0.7 m bgl) at Transect 1 and 2.

Location	θ (g/g)	Eh_F (mV)	pH_F	$Fe(II)_{HCl}:Fe_R$
Transect 1				
20 m	0.47 ±0.16	143 ±101	5.79 ±0.7	0.41 ±0.17
60 m	0.79 ±0.73	134 ±93	5.54 ±0.8	0.56 ±0.16
100 m	0.99 ±0.88	17 ±92	6.11 ±0.6	0.63 ±0.08
Transect 2				
20 m	0.33 ±0.15	590 ±64	4.43 ±0.1	0.04 ±0.03
40 m	0.43 ±0.14	531 ±219	4.08 ±1.3	0.07 ±0.08
60 m	0.58 ±0.05	277 ±207	5.05 ±1.2	0.18 ±0.09
80 m	0.79 ±0.09	158 ±157	5.86 ±0.7	0.23 ±0.10
100 m	0.84 ±0.15	168 ±73	5.94 ±0.5	0.28 ±0.11

Table SI 2. Relative proportion of As(III) in porewaters (mean ±standard deviation) at Transect 1, between 0.2 m to 1.0 m depth bgl.

Distance (m)	Mean As(III) (%)	*n*
30	87 ±20	5
60	81 ±21	4
110	82 ±15	9